frontiers | Frontiers in Physics

ORIGINAL RESEARCH
published: 09 May 2022
doi: 10.3389/fphy.2022.892581

Three-Dimensional Manipulation for Self-Focusing Behavior *via* the State of Polarization

Lu Lu[1†], *Zhiqiang Wang*[2,3†], *Rong Lin*[4] *and Yangjian Cai*[5,6*]

[1]Jiangsu Key Lab of Opto-Electronic Technology, School of Physics and Technology, Nanjing Normal University, Nanjing, China, [2]National Astronomical Observatories/Nanjing Institute of Astronomical Optics & Technology, Chinese Academy of Sciences, Nanjing, China, [3]CAS Key Laboratory of Astronomical Optics & Technology, Nanjing Institute of Astronomical Optics & Technology, Nanjing, China, [4]College of Physics and Electronic Engineering, Heze University, Heze, China, [5]Shandong Provincial Engineering and Technical Center of Light Manipulations & Shandong Provincial Key Laboratory of Optics and Photonic Device, School of Physics and Electronics, Shandong Normal University, Jinan, China, [6]School of Physical Science and Technology, Soochow University, Suzhou, China

In this work, the controllable self-focusing behavior is first investigated by manipulating the state of polarization (SoP), that is, the phase difference between two polarized components at the initial optical field, which can be used to realize the three-dimensional manipulation of self-focusing behavior. Furthermore, the properties of self-focusing propagation (including intensity distribution, propagation dynamics, and Stokes parameters) are researched in detail, which are beneficial to select the reasonable initial SoP for further theoretical and experimental exploration. Particularly, the radially polarized beam as a laser source not only prolongs the self-focusing length but also improves the power density of self-focusing spots on the target. These findings may have potential in the multidimensional optical manipulation, the optical information transmission, the high-power long-range laser atmospheric propagation, and related applications.

Keywords: self-focusing length, state of polarization, 3D manipulation, propagation characteristics, Stokes parameters

OPEN ACCESS

Edited by:
Shiyao Fu,
Beijing Institute of Technology, China

Reviewed by:
Xianfeng Chen,
Shanghai Jiao Tong University, China
Jianming Wen,
Kennesaw State University,
United States

***Correspondence:**
Yangjian Cai
yangjiancai@suda.edu.cn

†These authors have contributed equally to this work

Specialty section:
This article was submitted to Optics and Photonics, a section of the journal Frontiers in Physics

Received: *09 March 2022*
Accepted: *30 March 2022*
Published: *09 May 2022*

Citation:
Lu L, Wang Z, Lin R and Cai Y (2022) Three-Dimensional Manipulation for Self-Focusing Behavior via the State of Polarization. Front. Phys. 10:892581. doi: 10.3389/fphy.2022.892581

INTRODUCTION

In recent decades, filamentation propagation in the transparent medium [1], which can generate long plasma channels with very high intensities, has sparked extensive interest, owing to its wide application in many fields [2–5], such as lightening control, remote diagnostics, and LIDAR. In general, the filament length of laser pulse in the air is in the order of several meters to kilometers. In particular, the self-focusing length (SFL) plays a crucial role in high-power and long-range propagation [6–10] because it can make the length of filament steerable. Until now, the known methods for controlling the position of the filamentation domain are as follows: modulating the laser pulse power [6], adjusting the divergence angle of the initial laser [7], launching negatively chirped ultrashort pulses [8, 9], and double-lens setup [10]. Recently, the U.S. Naval Research Laboratory has investigated the SFL in atmospheric turbulence with theoretical and numerical methods [11, 12].

The vector optical field was proposed in 1961 [13]. Since 2000, this kind of optical field has been reappearing in sight due to its tight-focusing property [14]. The vector optical field with spatially inhomogeneous SoP at the field cross section has attracted immense attention, which can be widely used in nonlinear optics [15], optical tweezers [16], optical micro-manipulation [17], super-resolution microscopy [18], optical information transmission [19], and atmospheric propagation

[20–25]. In recent years, to conveniently control the space-variant polarization state of a light beam, the optical arrangements containing spatial light modulators have been widely presented [26–38]. Due to the axial-symmetry breaking of optical field by the designable hybrid polarization structure, i.e., azimuthally-variant hybrid-polarized (AVHP) vector field, the controllable self-focusing spots of the vector optical field and multiple filamentation have been achieved [36–38], which may provide an alternative solution to control the SFL. It is well-known that the SFL for a Gaussian beam is relevant with the input power, which can be described by the semi-empirical Marburger formula [9, 39, 40]. Due to the changeable intensity profile in propagation for a hollow beam (e.g., hollow Gaussian beam (HGB)), it is difficult to derive a formula to characterize the relation between the SFL and input power. As a typical kind of hollow beam, the radially polarized beam (RPB) has been studied extensively in both the theory and experiment, owing to its interesting and unique focusing properties [41–44]. Thus, a new method to achieve the controllable SFL of other common beams is worthy of further exploration as well.

In this work, based on the SoP manipulation, the influence of the phase difference at the initial optical field on the self-focusing propagation is researched. It is found that self-focusing behavior can be controlled by adjusting the phase difference, enabling a three-dimensional (3D) manipulation of the SFL. Furthermore, characteristics of self-focusing are investigated in detail by means of three specific beams (HGB, RPB, and AVHP). Results show that RPB have a predominant advantage in the controllable SFL and high optical power density on the target, and it may have practical application significance in the multidimensional optical manipulation, optical information transmission, high-power long-range laser atmospheric propagation, and related areas.

THEORY

We discussed the monochromatic (or continuous) regime for which the intensity of the laser does not depend on time. The propagation nonlinear dynamics of a high-power laser beam in the Kerr medium is researched by using nonlinear Schrödinger (NLS) equations. Under the slowly varying amplitude approximation, the NLS equation is given as follows[45, 46].

$$2ik\frac{\partial \mathbf{E}}{\partial z} + \nabla^2\mathbf{E} + \frac{4n_2k^2}{3n_0}\left[2(\mathbf{E}\cdot\mathbf{E}^*)\mathbf{E} + (\mathbf{E}\cdot\mathbf{E})\mathbf{E}^*\right] = 0, \quad (1)$$

where $\mathbf{E} = \mathbf{E}_0\exp(ikz)$, the wavenumber related to the wavelength is $k = 2\pi/\lambda$, $\nabla^2 = \partial^2/\partial r^2 + (1/r)\partial/\partial r + (1/r^2)\partial^2/\partial\varphi^2$ is the transverse Laplacian, n_0 (n_2) is the linear (nonlinear) refractive index, and ($*$) is the complex conjugate.

The azimuthally varying distribution of SoP at the initial optical field cross section can be expressed as follows [26, 35, 37].

$$\mathbf{E}(r,\varphi,z=0) = A(\mathbf{r})\left(\cos\delta\vec{\mathbf{e}}_x + \sin\delta\exp(-i\Delta\theta)\vec{\mathbf{e}}_y\right), \quad (2)$$

where $A(\mathrm{r}) = A_0(r/w_0)\exp(-\mathrm{r}^2/2w_0^2)$, A_0 is a normalized constant, w_0 is the beam waist associated with Gaussian beam, additional phase distribution δ is the function of the azimuthal angle φ as $\delta = m\varphi + \varphi_0$, m is the topological charge, and φ_0 is the initial phase [35]. $\vec{e}_x$ and $\vec{e}_y$ are the unit vectors in the Cartesian coordinate system, which describe the linearly polarized fields with their directions of vibration along the x and y axes [35]. $\Delta\theta$ is the phase difference between the x and y polarized components in the range of $\Delta\theta \in [0,\pi]$ [26, 35]. It is clear that **Eq. 2** can be simplified to several specific cases as follows:

i) when $\delta = 0$ and $\Delta\theta = 0$, the linearly polarized states are along the x-axis (**Figure 1A**), and **Eq. 2** is regarded as a scalar optical field, i.e., HGB [47],

$$\mathbf{E}(r,\varphi,z=0) = A(\mathbf{r})\vec{\mathbf{e}}_x. \quad (3)$$

(ii) when $\delta \neq 0$ and $\Delta\theta = 0$, the linearly polarized states are at any position in the cross section (**Figure 1B**), and the RPB is represented as follows [36].

$$\mathbf{E}(r,\varphi,z=0) = A(\mathbf{r})\left(\cos\delta\vec{\mathbf{e}}_x + \sin\delta\vec{\mathbf{e}}_y\right). \quad (4)$$

(iii) when $\delta \neq 0$ and $\Delta\theta = \pi/2$, SoPs are distributed as follows, that is, 'linear→ elliptical→ circular→ elliptical →linear' (**Figure 1C**). The AVHP vector field is presented in [36] as

$$\mathbf{E}(r,\varphi,z=0) = A(\mathbf{r})\left(\cos\delta\vec{\mathbf{e}}_x + \sin\delta\exp(-i\pi/2)\vec{\mathbf{e}}_y\right), \quad (5)$$

The vector NLS equation can be divided into a pair of coupled NLS equations for two orthogonal components,

$$\begin{aligned} 2ik\frac{\partial E_x}{\partial z} + \nabla^2E_x + \frac{4n_2k^2}{3n_0}\left[3|E_x|^2E_x + 2|E_y|^2E_x + E_y^2E_x^*\right] = 0,\\ 2ik\frac{\partial E_y}{\partial z} + \nabla^2E_y + \frac{4n_2k^2}{3n_0}\left[3|E_y|^2E_y + 2|E_x|^2E_y + E_x^2E_y^*\right] = 0, \end{aligned} \quad (6)$$

where E_x (E_y) is the x- or y-component of the optical field.

The SoP of the optical field cross section can be described by a set of Stokes parameters. Stokes polarization parameters are expressed as follows [48]:

$$\begin{aligned} S_0 &= |E_x|^2 + |E_y|^2,\\ S_1 &= |E_x|^2 - |E_y|^2,\\ S_2 &= E_xE_y^* + E_yE_x^*,\\ S_3 &= i\left(E_xE_y^* - E_yE_x^*\right), \end{aligned} \quad (7)$$

where the positive and negative S_1 (or S_2) values represent horizontal (or 45°) and vertical (or 135°) linear polarization components, respectively; positive and negative S_3 values represent opposite circular components [37].

THREE-DIMENSIONAL MANIPULATION OF SELF-FOCUSING BEHAVIOR *VIA* SOPS

In the numerical calculation, the initial parameters are chosen as follows: wavelength $\lambda = 0.532$ μm, step number $M = 2000$, linear

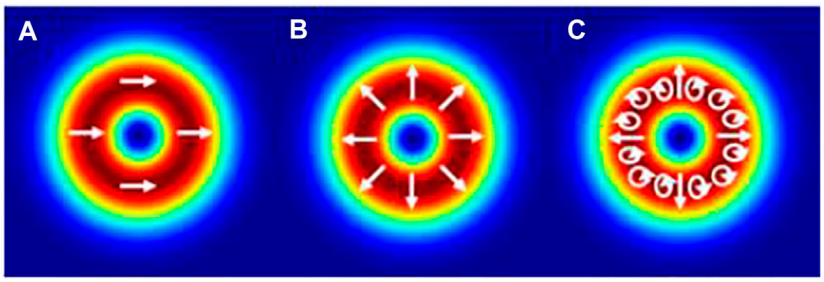

FIGURE 1 | Cross-section of the initial optical field: **(A)** HGB, **(B)** RPB, and **(C)** AVHP.

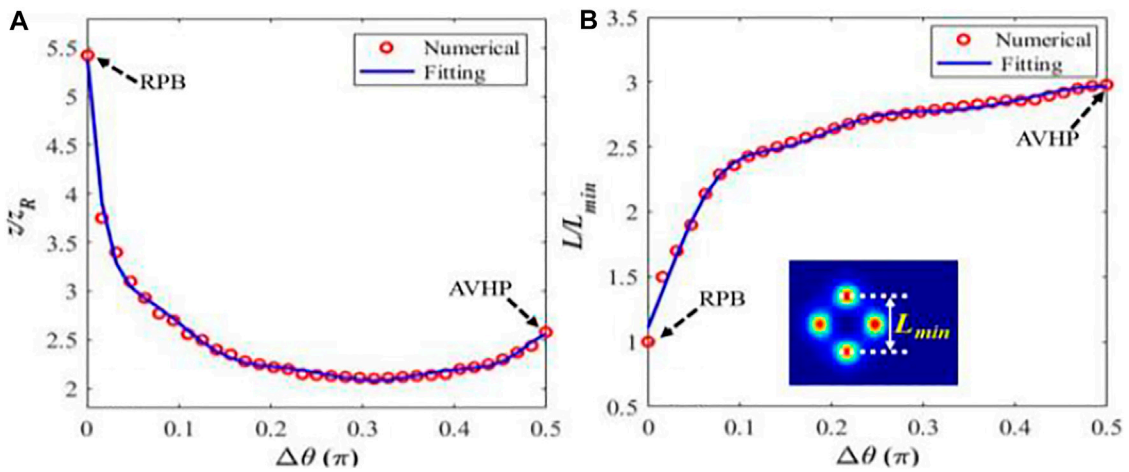

FIGURE 2 | SFL **(A)** and spacing **(B)** of self-focusing spots versus the phase difference.

refractive index of medium $n_0 = 1$, nonlinear refractive index $n_2 = 5 \times 10^{-23}$ m^2/W, propagation length $z = C{*}z_R$ (C is a constant, and Rayleigh length is $z_R = \pi w_0^2/\lambda$), transverse size $10w_0$, grid number $N = 512$, andP_{cr} is the critical power of a Gaussian beam model for self-focusing. The numerical results are obtained by the fast Fourier transform Runge–Kutta split-step method [49].

It is known that adjusting the input power is a common method to manipulate the SFL for a Gaussian beam [6]. For three hollow beams, the numerical relation of the SFL the with input power is shown in detail in **Supplementary Material S1**. However, in the practical experimental scenario, as an alternative or combination regimen to the input power manipulation, the approach to achieve the controllable SFL at the fixed input power is still a great challenge, which may greatly extend the manipulation dimensionality. As an intrinsic nature of light, polarization is of great importance to serve as a degree of freedom for manipulating light. With the aid of SoPs, herein, the manipulation of beam collapse under fixed input power is explored, that is, input power $P = 30P_{cr}$, topological charge $m = 1$, and initial phase $\varphi_0 = 0$ are considered, and the extension to other input power (topological charge, beam waist, wavelength, etc.) is straightforward. In previous studies [9, 40], there is an expression for the SFL where the size of the focusing spot reaches zero. Due to the initial optical field cross section with spatially inhomogeneous SoP, the relationship between the SFL and the phase difference will be much more complicated. To simplify the problem, the minimum radius of the focusing spot is approximated to 7.5 μm in numerical calculation (i.e., approximately 7.5% of the initial beam radius $w_0 = 100$ μm); thus, the propagation length can be approximately regarded as the SFL. The phase difference in **Figure 2** is selected from 0 to $\pi/2$, and the interval is $\pi/64$. In **Figure 2A**, the SFL is plotted as a function of the phase difference. It is shown that the SFL is continuously adjustable in the range of 2.1–5.4 times of the

TABLE 1 | Coefficients of the fitting function versus phase difference.

	$i = 1$	$i = 2$	$i = 3$	$i = 4$	$i = 5$
a_i	5.11×10^{13}	1.38×10^{11}	0.62	8.40	3.56
b_i	−1.31	1.89	0.50	2.19	−0.38
c_i	0.23	0.18	0.13	1.17	0.70
p_i	2.88	1.59	1.59	0.91	0.91
q_i	0.50	0.82	0.19	0.06	0.94
t_i	0.29	0.16	0.16	0.08	0.08

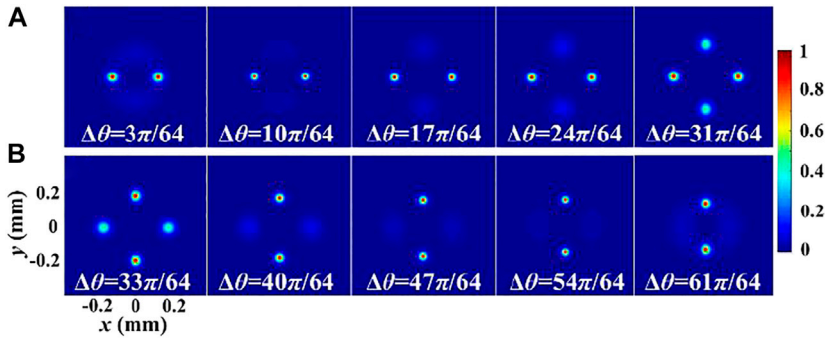

FIGURE 3 | Intensity distribution of self-focusing spots with various phase differences: **(A)** $\Delta\theta \in (0, \pi/2)$and **(B)** $\Delta\theta \in (\pi/2, \pi)$, respectively.

Rayleigh length, which may have a practical application significance for the SFL manipulation in the axial dimensionality. In addition, results of the SFL for $\Delta\theta \in [\pi/2, \pi]$ and $\Delta\theta \in [0, \pi/2]$ are symmetric at $\Delta\theta = \pi/2$. Based on the numerical calculation of the SFL and a Gaussian model for curve fitting, the numerical formula of the SFL varying with the phase difference can be expressed as $z = z_R \times \sum_{i=1}^{5} a_i \exp\{-[(\Delta\theta - b_i)/c_i]^2\}$, and the corresponding coefficients are listed in the **Table 1**.

Next, the spacing of symmetric self-focusing spots at the collapse plane is investigated. Herein, the minimum value $L_{\min}$ is defined as the spacing of symmetric self-focusing spots for the RPB case (**Figure 2B**). The result shows that the spacing of the two spots increases as the phase difference increases within the range of $\Delta\theta \in [0, \pi/2]$, and this spacing can be controlled approximately from $L_{\min}$ to $3L_{\min}$, which indicates that the radial dimensionality of self-focusing spots can be adjusted as well. When $\Delta\theta \in [\pi/2, \pi]$, the result is axisymmetric at $\Delta\theta = \pi/2$ that the spacing gradually decreased as phase difference increased. Using the aforementioned method of the SFL, the numerical formula of the spacing of self-focusing spots with the phase difference can be expressed as $L = L_{\min} \times \sum_{i=1}^{5} p_i \exp\{-[(\Delta\theta - q_i)/t_i]^2\}$, and the coefficients are exhibited in **Table 1**.

The intensity distribution of self-focusing spots is illustrated in **Figure 3**, where the phase differences are changed in two regions, i.e., $\Delta\theta \in (0, \pi/2)$ and $\Delta\theta \in (\pi/2, \pi)$, and the interval of the phase difference is $7\pi/64$. By increasing the phase difference in $(0, \pi/2)$, spacing of self-focusing spots increases, and the number tends to increase. When the phase difference changes from $\pi/2$ to π, the number of spots decreases and the orientation rotates by $\pi/2$. It is shown that the number and orientation of self-focusing spots can be controlled by changing the phase difference so that the azimuthal dimensionality of self-focusing can be manipulated to some extent.

Based on the variation of the phase difference, the fine manipulation of self-focusing spots (including the length, spacing, number, and orientation) can be achieved. It is found that manipulation of SoPs can be controlled not only in the axial dimensionality (i.e., the SFL) but also in radial (i.e., the spacing of self-focusing spots) and azimuthal (i.e., the number and orientation of self-focusing spots) dimensionalities. To the best of our knowledge, this is the first time to achieve three-dimensional (3D) manipulation of self-focusing behavior simultaneously by changing the phase difference. Meanwhile, the extension of this concept to other initial parameters (i.e., the input power, beam waist, wavelength, and nonlinear refractive index) is straightforward, and the limitations will be discussed in *Conclusion and Discussion*. Combining the manipulation of the input power and phase difference, it may enrich the multidimensional manipulation for self-focusing, which may provide a new approach to realizing the 3D manipulation of the optical field, enhancing the optical information transmission capacity, improving the high-power long-range atmospheric shooting on the target, and related areas.

CHARACTERISTICS OF SELF-FOCUSING

To analyze the physical mechanism of the self-focusing propagation, the characteristics of the self-focusing spot for three specific beams are investigated in detail with the help of the intensity distribution, propagation dynamics, and Stokes parameters. The parameters in numerical calculation are the same as the aforementioned section.

The intensity distribution at different propagation planes and propagation dynamics of three optical fields are shown in **Figure 4**. At the source plane $z = 0$, the intensity distribution for three cases is almost the same, that is, a typical symmetric ring. However, the discrepancy of the intensity distribution in the three cases increases gradually with the increase of the propagation distance. For the HGB (i.e., **Figure 4A**), the dark center almost disappears at Rayleigh length z_R. Due to the propagation property of the HGB and the self-focusing effect of the medium, the Gaussian beam shrinks to a single spot at $z = 1.6z_R$. For the RPB (i.e., **Figure 4B**), the hollow beam shape remains, except that the width of the ring decreases at z_R. With the propagation distance increased, the hollow beam collapses and converges into four spots at $z = 5.4z_R$. For the AVHP (i.e., **Figure 4C**), the hollow shape gradually disappears, and energy converges toward four linear polarization locations at z_R. The axial symmetry of the light-matter nonlinear interaction is broken by the designable

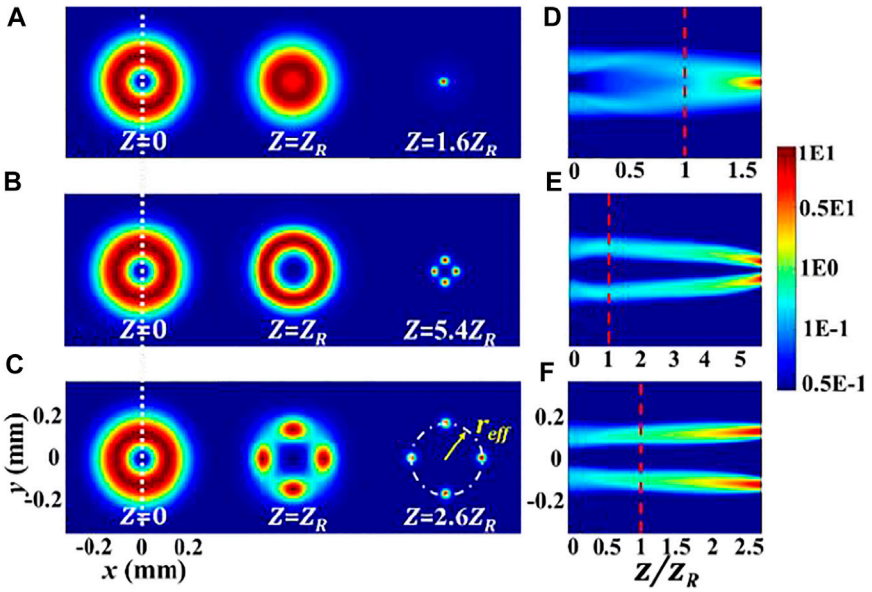

FIGURE 4 | Intensity distribution located at various propagation planes for three optical fields **(A)** HGB, **(B)** RPB, and **(C)** AVHP and the corresponding propagation dynamics **(D–F)**, respectively.

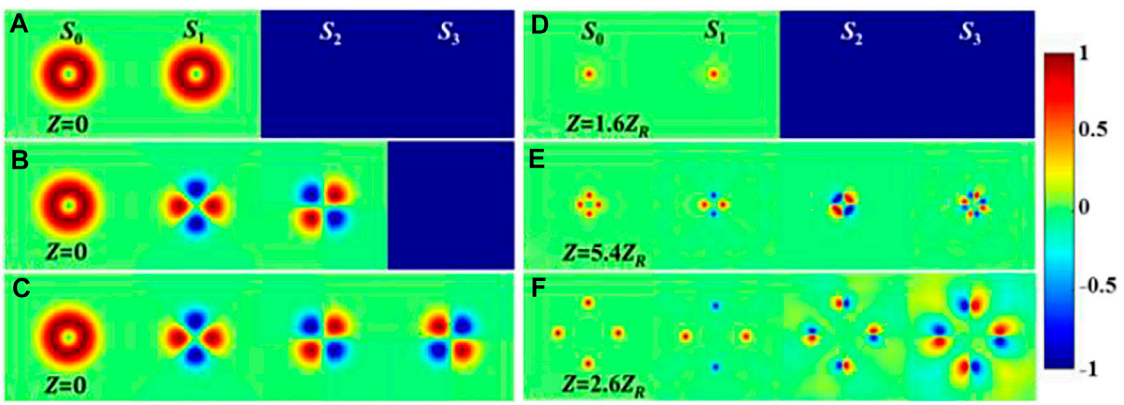

FIGURE 5 | Stokes polarization parameters for three beam models at the source plane (i.e., **(A)** HGB, **(B)** RPB, and **(C)** AVHP) and at the corresponding focusing spot (i.e., **(D)** HGB ($z = 1.6z_R$), **(E)** RPB ($z = 5.4z_R$), and **(F)** AVHP ($z = 2.6z_R$)).

hybrid polarization structure at the initial optical field cross section, and then, four deterministic self-focusing spots occur at $z = 2.6z_R$. Owing to the symmetry, a crossline (i.e., $x = 0$) of the intensity distribution is chosen to demonstrate propagation dynamics for three models. As shown in **Figures 4D–F**, the SFL in three models satisfy the following relation: RPB > AVHP > HGB. HGB forms a single spot while the vector beam generates four spots for $m = 1$; the power of the RPB on the target is almost four times higher than that of the HGB [37, 50, 51]. Moreover, the effective radius of the RPB is smaller than that of AVHP, which indicates that the power density of the RPB is larger than that of the AVHP. It is possible that the RPB as a laser source may be of great advantage to achieve the long-range and high-power laser atmospheric propagation, far-field optical engineering [52, 53], and optical coherence encryption [54].

Stokes parameters for three models at the source plane (**Figures 5A–C**) and the corresponding spot plane (**Figure 5D–F**) are depicted, which benefits to analyze the physical mechanism of the self-focusing behavior. Stokes parameters for the HGB are shown in **Figure 5A,D**; it is seen that S_2 or S_3 remains the same as the propagation distance increases. Owing to the propagation property of the HGB and the self-focusing effect of the medium, the self-focusing spot occurs in the center. The RPB shown in **Figures 5B,E** indicates that there is no circular polarization ($S_3 = 0$) at the source plane, while the circular polarization

states occur on the spot plane because the Stokes parameter S_3 is not equal to zero. It is clear that the hybrid polarization spatial structure is formed during the propagation process, so the symmetry is broken by the refractive index change; four self-focusing spots are located at $x = 0$ and $y = 0$ lines as expected. The AVHP shown in **Figures 5C,F** indicates that spots move to the linear polarization locations because the symmetry of the light-matter nonlinear interaction is broken by the designable hybrid polarization structure at the cross section of the initial optical field [55].

CONCLUSION AND DISCUSSION

Based on the phase difference between two polarized components at the initial optical field cross section, the influence of the phase difference on self-focusing behavior is investigated. It is found that the length, spacing, number, and orientation of self-focusing spots can be controlled by adjusting the phase difference. In particular, it is of practical significance for realizing the 3D manipulation of self-focusing behavior simultaneously by changing the phase difference. In addition, properties of the SFL are investigated in detail with three specific models (i.e., HGB, RPB, and AVHP). It is revealed that the SFL of three cases satisfies the following relation: RPB > AVHP > HGB. In addition, two characteristics for the RPB should be mentioned: 1) self-focusing spots appear at a relatively long-range propagation distance; 2) the target optical power density of the RPB is larger than that of the AVHP at the receiver plane due to the effective beam radius focusing. Therefore, the RPB as a laser source may not only prolong the SFL but also improve the power density on the target. Based on the multidimensional controllable manipulation by changing the SoPs, it may open a new window for realizing the applications, such as 3D manipulation of the optical field, the optical information transmission, and the high-power long-range atmospheric propagation.

An extension of these results to other initial parameters (i.e., the input power, beam waist, wavelength, and nonlinear refractive index) is straightforward with reasonable limitations on some parameters. When the input power of the laser is much greater than the critical power, the beam may break up into multiple spots, forming its own filament with the critical power [37, 50, 51]. In our work, we discussed the relation of the SFL with moderate input power and the input power, which can generate four spots for the vector optical field that should be at least larger than four times of critical power: $P > 4P_{cr}^{A} = 19.2P_{cr}$. When the nonlinear refractive index approaches the linear refractive index, the aforementioned extension will be invalid due to the large variation of the refractive index. The values of the nonlinear refractive index are relatively small for many media, taking air for example, the wavelength at 532 nm (or 800 nm) is corresponding to $n_2 = 5 \times 10^{-23}$ m^2/W (or $n_2 = 3.0 \times 10^{-23}$ m^2/W [56]).

For the conventional physical mechanism of multiple filamentation (MF), when the input peak power is far above the critical power for self-focusing, the modulational instability breaks up the beam into a large number of filaments [1]. These filaments, which grow from the small fluctuations in the beam intensity profile, can be seemingly randomly distributed in a given transverse plane or organized into specific patterns, and the number of filaments cannot be accurately predicted [1]. For the multiple spots induced by SoPs, a prerequisite is that the optical field should be axial-symmetry breaking in and of itself. Polarization, as an intrinsic and fundamental nature of light, plays an indispensable role in the interaction of light with matter. The self-focusing spot formation mechanism is axial-symmetry breaking [36, 37] due to the inhomogeneous state of polarization at the initial optical field cross section or the induction of the propagation process. With the input power changed, the distribution of spots is predictable, and the number also can be determined. Thus, these theoretical and numerical findings may be achieved by the controllable self-focusing behavior, and it may have practical application significance in 3D optical manipulation, optical information transmission, high-power long-range laser atmospheric propagation, and so on.

DATA AVAILABILITY STATEMENT

The original contributions presented in the study are included in the article/**Supplementary Material**, further inquiries can be directed to the corresponding author.

AUTHOR CONTRIBUTIONS

All authors listed have made a substantial, direct, and intellectual contribution to the work and approved it for publication.

ACKNOWLEDGMENTS

We acknowledge the National Key Research and Development Project of China (2019YFA0705000), the National Natural Science Foundation of China (12192254, 91750201, 11974218, 11804234, 11903062, and 11904087), the Innovation Group of Jinan (2018GXRC010), and the Local Science and Technology Development Project of the Central Government (YDZX20203700001766).

SUPPLEMENTARY MATERIAL

The Supplementary Material for this article can be found online at: https://www.frontiersin.org/articles/10.3389/fphy.2022.892581/full#supplementary-material

REFERENCES

1. Couairon A, Mysyrowicz A. Femtosecond Filamentation in Transparent Mediafilamentation in Transparent media. *Phys Rep* (2007) 441:47–189. doi:10.1016/j.physrep.2006.12.005
2. Kasparian J, Rodriguez M, Me´jean G, Yu J, Salmon E, Wille H, et al. White-light Filaments for Atmospheric Analysis. *Science* (2003) 301:61–4. doi:10.1126/science.1085020
3. Houard A, D'Amico C, Liu Y, André YB, Franco M, Prade B, et al. High Current Permanent Discharges in Air Induced by Femtosecond Laser Filamentation. *Appl Phys Lett* (2007) 90:171501. doi:10.1063/1.2734396
4. D'Amico C, Houard A, Franco M, Prade B, Mysyrowicz A, Couairon A, et al. Conical Forward THz Emission from Femtosecond-Laser-Beam Filamentation in Air. *Phys Rev Lett* (2007) 98:235002. doi:10.1103/PhysRevLett.98.235002
5. Amico CD, Houard A, Akturk S, Liu Y, Le Bloas J, Franco M, et al. Forward THz Radiation Emission by Femtosecond Filamentation in Gases: Theory and experiment. *New J Phys* (2008) 10:013015. doi:10.1088/1367-2630/10/1/013015
6. Houard A, Franco M, Prade B, Durécu A, Lombard L, Bourdon P, et al. Femtosecond Filamentation in Turbulent Air. *Phys Rev A* (2008) 78:033804. doi:10.1103/physreva.78.033804
7. Jin Z, Zhang J, Xu MH, Lu X, Li YT, Wang ZH, et al. Control of Filamentation Induced by Femtosecond Laser Pulses Propagating in Air. *Opt Express* (2005) 13(25):10424–30. doi:10.1364/opex.13.010424
8. Wöste L, Wedekind C, Wille H, Rairoux P, Stein B, Nikolov S, et al. Femtosecond Atmospheric Lamp. *Laser und Optoelektronik*. AT specialist Publisher (1997).
9. Sprangle P, Peñano JRB, Hafizi B. Propagation of Intense Short Laser Pulses in the Atmosphere. *Phys Rev E Stat Nonlin Soft Matter Phys* (2002) 66:046418. doi:10.1103/PhysRevE.66.046418
10. Fibich G, Sivan Y, Ehrlich Y, Louzon E, Fraenkel M, Eisenmann S, et al. Control of the Collapse Distance in Atmospheric Propagation. *Opt Express* (2006) 14(12):4946–57. doi:10.1364/oe.14.004946
11. Stotts LB, Peñano J, Urick VJ. Engineering Equation for Filamentation Self-Focusing Collapse Distance in Atmospheric Turbulence. *Opt Express* (2019) 27(11):15159–71. doi:10.1364/oe.27.015159
12. DiComo G, Helle M, Kaganovich D, Schmitt-Sody A, Elle J, Peñano J. Nonlinear Self-Channeling of High-Power Lasers through Controlled Atmospheric Turbulence. *J Opt Soc Am B* (2020) 37(3):797–803. doi:10.1364/josab.384137
13. Snitzer E. Cylindrical Dielectric Waveguide Modes*. *J Opt Soc Am* (1961) 51(5):491–8. doi:10.1364/josa.51.000491
14. Youngworth KS, Brown TG. Focusing of High Numerical Aperture Cylindrical-Vector Beams. *Opt Express* (2000) 7(2):77–87. doi:10.1364/oe.7.000077
15. Ciattoni A, Crosignani B, Di Porto PA, Yariv A. Azimuthally Polarized Spatial Dark Solitons: Exact Solutions of Maxwell's Equations in a Kerr Medium. *Phys Rev Lett* (2005) 94(7):073902. doi:10.1103/PhysRevLett.94.073902
16. Kawauchi H, Yonezawa K, Kozawa Y, Sato S. Calculation of Optical Trapping Forces on a Dielectric Sphere in the ray Optics Regime Produced by a Radially Polarized Laser Beam. *Opt Lett* (2007) 32(13):1839–41. doi:10.1364/ol.32.001839
17. Lou K, Qian S-X, Wang X-L, Li Y, Gu B, Tu C, et al. Two-dimensional Microstructures Induced by Femtosecond Vector Light fields on Silicon. *Opt Express* (2012) 20(1):120–7. doi:10.1364/oe.20.000120
18. Xie X, Chen Y, Yang K, Zhou J. Harnessing the point-spread Function for High-Resolution Far-Field Optical Microscopy. *Phys Rev Lett* (2014) 113:263901. doi:10.1103/physrevlett.113.263901
19. Gao X-Z, Pan Y, Zhao M-D, Zhang G-L, Zhang Y, Tu C, et al. Focusing Behavior of the Fractal Vector Optical fields Designed by Fractal Lattice Growth Model. *Opt Express* (2018) 26(2):1597–614. doi:10.1364/oe.26.001597
20. Cai Y, Lin Q, Eyyuboglu HT, Baykal Y. Average Irradiance and Polarization Properties of a Radially or Azimuthally Polarized Beam in a Turbulent Atmosphere. *Opt Express* (2008) 16(11):7665–73. doi:10.1364/oe.16.007665
21. Cheng W, Haus JW, Zhan Q. Propagation of Vector Vortex Beams through a Turbulent Atmosphere. *Opt Express* (2009) 17(20):17829–36. doi:10.1364/oe.17.017829
22. Wei C, Wu D, Liang C, Wang F, Cai Y. Experimental Verification of Significant Reduction of Turbulence-Induced Scintillation in a Full Poincaré Beam. *Opt Express* (2015) 23(19):24331–41. doi:10.1364/oe.23.024331
23. Cox MA, Rosales-Guzmán C, Lavery MPJ, Versfeld DJ, Forbes A. On the Resilience of Scalar and Vector Vortex Modes in Turbulence. *Opt Express* (2016) 24(16):18105–13. doi:10.1364/oe.24.018105
24. Lavery MPJ, Peuntinger C, Günthner K, Banzer P, Elser D, Boyd RW, et al. Free-space Propagation of High-Dimensional Structured Optical fields in an Urban Environment. *Sci Adv* (2017) 3(10):e1700552. doi:10.1126/sciadv.1700552
25. Yu J, Huang Y, Wang F, Liu X, Gbur G, Cai Y. Scintillation Properties of a Partially Coherent Vector Beam with Vortex Phase in Turbulent Atmosphere. *Opt Express* (2019) 27:26676. doi:10.1364/oe.27.026676
26. Han W, Yang Y, Cheng W, Zhan Q. Vectorial Optical Field Generator for the Creation of Arbitrarily Complex fields. *Opt Express* (2013) 21(18):20692–706. doi:10.1364/oe.21.020692
27. Han W, Cheng W, Zhan Q. Design and Alignment Strategies of 4f Systems Used in the Vectorial Optical Field Generator. *Appl Opt* (2015) 54(9):2275–8. doi:10.1364/ao.54.002275
28. Wan C, Zhan Q. Generation of Exotic Optical Polarization Möbius Strips. *Opt Express* (2019) 27(8):11516–24. doi:10.1364/oe.27.011516
29. Stirling S, Hend S, Kamel A, Zhan Q, Andrew F. General Design Principle for Structured Light Lasers. *Opt Express* (2020) 28(23):35006–17. doi:10.1364/oe.410963
30. Liu S, Qi S, Zhang Y, Li P, Wu D, Han L, et al. Highly Efficient Generation of Arbitrary Vector Beams with Tunable Polarization, Phase, and Amplitude. *Photon Res* (2018) 6(4):228–33. doi:10.1364/prj.6.000228
31. Ma C, Di J, Zhang Y, Li P, Xiao F, Liu K, et al. Reconstruction of Structured Laser Beams through a Multimode Fiber Based on Digital Optical Phase Conjugation. *Opt Lett* (2018) 43(14):3333–6. doi:10.1364/ol.43.003333
32. Ma C, Di J, Dou J, Li P, Xiao F, Liu K, et al. Structured Light Beams Created through a Multimode Fiber via Virtual Fourier Filtering Based on Digital Optical Phase Conjugation. *Appl Opt* (2020) 59(3):701–5. doi:10.1364/ao.380058
33. Chen Z, Zeng T, Qian B, Ding J. Complete Shaping of Optical Vector Beams. *Opt Express* (2015) 23(14):17701–10. doi:10.1364/oe.23.017701
34. Li L, Chang C, Yuan C, Feng S, Nie S, Ren Z-C, et al. High Efficiency Generation of Tunable Ellipse Perfect Vector Beams. *Photon Res* (2018) 6(12):1116–23. doi:10.1364/prj.6.001116
35. Wang H-T, Wang X-L, Li Y, Chen J, Ding C-SJ, Wang H. A New Type of Vector fields with Hybrid States of Polarization. *Opt Express* (2010) 18:10786–95. doi:10.1364/oe.18.010786
36. Li S-M, Li Y, Wang X-L, Kong L-J, Lou K, Tu C, et al. Taming the Collapse of Optical Fields. *Sci Rep* (2012) 2:1007. doi:10.1038/srep01007
37. Chen R-P, Zhong L-X, Chew K-H, Zhao T-Y, Zhang X. Collapse Dynamics of a Vector Vortex Optical Field with Inhomogeneous States of Polarization. *Laser Phys* (2015) 25:075401. doi:10.1088/1054-660x/25/7/075401
38. Li S-M, Ren Z-C, Kong L-J, Qian S-X, Tu C, Li Y, et al. Unveiling Stability of Multiple Filamentation Caused by Axial Symmetry Breaking of Polarization. *Photon Res* (2016) 4:B29–B34. doi:10.1364/prj.4.000b29
39. Marburger JH, Dawes E. Dynamical Formation of a Small-Scale Filament. *Phys Rev Lett* (1968) 21:556–8. doi:10.1103/physrevlett.21.556
40. Peñano J, Hafizi B, Ting A, Helle M. Theoretical and Numerical Investigation of Filament Onset Distance in Atmospheric Turbulence. *J Opt Soc Am B* (2014) 31(5):963–71. doi:10.1364/josab.31.000963
41. Wu G, Wang F, Cai Y. Coherence and Polarization Properties of a Radially Polarized Beam with Variable Spatial Coherence. *Opt Express* (2012) 20(27):28301–18. doi:10.1364/oe.20.028301
42. Wang F, Cai Y, Dong Y, Korotkova O. Experimental Generation of a Radially Polarized Beam with Controllable Spatial Coherence. *Appl Phys Lett* (2012) 100:051108. doi:10.1063/1.3681802
43. Zhu S, Wang J, Liu X, Cai Y, Li Z. Generation of Arbitrary Radially Polarized Array Beams by Manipulating Correlation Structure. *Appl Phys Lett* (2016) 109:161904. doi:10.1063/1.4965705

44. Ping C, Liang C, Wang F, Cai Y. Radially Polarized Multi-Gaussian Schell-Model Beam and its Tight Focusing Properties. *Opt Express* (2017) 25(26): 32475–90. doi:10.1364/oe.25.032475
45. Menyuk CR. Stability of Solitons in Birefringent Optical Fibers II Arbitrary Amplitudes. *J Opt Soc Am B* (1988) 5(2):392–402. doi:10.1364/josab.5.000392
46. Park Q-H, Shin HJ. Painlevé Analysis of the Coupled Nonlinear Schrödinger Equation for Polarized Optical Waves in an Isotropic Medium. *Phys Rev E* (1999) 59(2):2373–9. doi:10.1103/physreve.59.2373
47. Cai Y, Lu X, Lin Q. Hollow Gaussian Beams and Their Propagation Properties. *Opt Lett* (2003) 28:1084–6. doi:10.1364/ol.28.001084
48. Born M, Wolf E. *Principles of Optics*. 7th ed. Cambridge University Press (1999).
49. Dubietis A, Gaižauskas E, Tamošauskas G, Di Trapani P. Light Filaments without Self-Channeling. *Phys Rev Lett* (2004) 92:253903. doi:10.1103/physrevlett.92.253903
50. Wang D, Liu G-G, Lü J-Q, Li P-P, Cai M-Q, Zhang G-L, et al. Femtosecond Polarization-Structured Optical Field Meets an Anisotropic Nonlinear Medium. *Opt Express* (2018) 26(21):27726–47. doi:10.1364/oe.26.027726
51. Braun A, Korn G, Liu X, Du D, Squier J, Mourou G. Self-channeling of High-Peak-Power Femtosecond Laser Pulses in Air. *Opt Lett* (1995) 20:73–5. doi:10.1364/ol.20.000073
52. Liu Y, Chen Y, Chen Y, Wang F, Cai Y, Liang C, et al. Robust Far-Field Imaging by Spatial Coherence Engineering. *Opto-Electron. Adv* (2021) 4:210027. doi:10.29026/oea.2022.210027
53. Zhang X, Chen Y, Wang F, Cai Y. Scattering of Partially Coherent Vector Beams by a Deterministic Medium Having Parity-Time Symmetry. *Photonics* (2022) 9:140. doi:10.3390/photonics9030140
54. Peng D, Huang Z, Liu Y, Chen Y, Wang F, Ponomarenko SA, et al. Optical Coherence Encryption with Structured Random Light. *PhotoniX* (2021) 2:6. doi:10.1186/s43074-021-00027-z
55. Moll KD, Gaeta AL, Fibich G. Self-Similar Optical Wave Collapse: Observation of the Townes Profile. *Phys Rev Lett* (2003) 90:203902. doi:10.1103/physrevlett.90.203902
56. Geints YE, Kabanov AM, Zemlyanov AA, Bykova EE, Bukin OA, Golik SS. Kerr-driven Nonlinear Refractive index of Air at 800 and 400 Nm Measured through Femtosecond Laser Pulse Filamentation. *Appl Phys Lett* (2011) 99: 181114. doi:10.1063/1.3657774

Conflict of Interest: The authors declare that the research was conducted in the absence of any commercial or financial relationships that could be construed as a potential conflict of interest.